Correlations between the kinetics and the mechanisms of hot corrosion of pure nickel at 700 °C

Benjamin Grégoire, Xabier Montero, Mathias Galetz, Gilles Bonnet, Fernando Pedraza

Correlations between the kinetics and the mechanisms of hot corrosion of pure nickel at 700°C

Benjamin Grégoire[a,*], Xabier Montero[b], Mathias C. Galetz[b], Gilles Bonnet[a], Fernando Pedraza[a]

[a] *Laboratoire des Sciences de l'Ingénieur pour l'Environnement (LaSIE, UMR-CNRS 7356), La Rochelle Université, Avenue Michel Crépeau, 17042 La Rochelle Cedex 1, France*

[b] *DECHEMA-Forschungsinstitut, Theodor-Heuss-Allee 25, 60486 Frankfurt am Main, Germany*

* Corresponding author: benjamin.gregoire@univ-lr.fr

ABSTRACT

This study investigates the kinetics of hot corrosion of pure nickel exposed to different testing conditions at 700°C. Whereas nickel underwent pure oxidation when exposed to synthetic air only, the addition of 0.5% SO_2/SO_3 induced oxidation-sulphidation and considerably increased the corrosion kinetics. In the presence of sodium sulphate (Na_2SO_4), Ni-S liquid solutions systematically formed at the metal/scale interface. This was attributed to the shielding effect of Na_2SO_4 implying negative pO_2 and pSO_3 gradients from the gas/salt interface towards the scale/salt interface. The influence of thermal cycling as well as the testing method (i.e. half-embedding and salt-recoating) was also elucidated.

Keywords: nickel; hot corrosion; oxidation; sulphidation; kinetics

1. Introduction

The improved γ-γ' *duplex* microstructure of nickel-based superalloys provides high creep and fatigue resistance at elevated temperatures for gas turbine components. However, these materials are submitted to hot corrosive gases (O_2, H_2O, SO_2) and to the presence of diverse impurities under operation, which reduce their lifetime [1-5]. In specific conditions, salt mixtures can deposit on the surface of components leading to hot corrosion [6-8]. Depending on the temperature of the components, two modes of deposit-induced hot corrosion are usually considered in sodium sulphate (Na_2SO_4): Type-I at about 900°C (fused deposits) and Type-II at about 700°C (formation of eutectic mixtures, e.g. Na_2SO_4-$NiSO_4$ at 671°C, by interaction between the deposit and the underlying oxides) [6,7]. Since nickel constitutes the base-metal of many heat-resistant alloys, its oxidation, oxidation-sulphidation and deposit-induced hot corrosion behaviour has been thoroughly investigated over the past decades [9-17]. Its study might also be of interest for austenitic steels and nickel-based superalloys exposed to long-term hot corrosion exposure. Such long-term exposure provokes such protective elements depletion that the behaviour of the alloys resembles to that of pure nickel. The mechanisms of corrosion of nickel are usually assessed by metallographic observations and weight change measurements [10-12].

These mechanisms are particularly sensitive to the testing conditions (e.g. temperature, gas composition and salt deposit composition) and efforts have been made to better simulate real exposure conditions at laboratory scale. Even though weight change measurements are very often used to follow the kinetics of gas-phase induced corrosion and oxidation, this method does not appear applicable to describe deposit-induced hot corrosion since the microstructures usually reveal heterogeneous attack of the samples and fused deposits [2-4]. This is particularly true for Type-II hot corrosion conditions characterized by pitting [2,5,6].

Since the pioneer works of Pettit and collab. [18-20], it has long been acknowledged that the deposit-induced hot corrosion attack can be divided into two stages: incubation (or inititation) and propagation. During the incubation stage, the attack seems to be similar to that occurring in the absence of a deposit (i.e. reaction between the gas and the material). This stage usually ends when local attack of the material occurs by fluxing mechanisms or internal oxidation/sulphidation [7,18]. Several factors may influence the length of the incubation stage including the material composition, the temperature, the gas composition, the salt chemistry and thermal cycles. To follow the Type-II hot corrosion kinetics of industrial nickel-based superalloys, Cranfield University developed a corrosion model based upon the rate of metal loss (ML) in the incubation stage (k_{inc}), the rate of metal loss in the propagation stage (k_{prop}) and the incubation period (t_{inc}) defined as the time when there is a transition according to Eqs. **(1)** and **(2)** [2,5]:

$$ML = k_{inc}.t^m \quad \textbf{(1)}$$

$$ML = k_{inc}.t_{inc}^m + k_{prop}.(t-t_{inc})^n \quad \textbf{(2)}$$

Eq. **(1)** represents the incubation stage and Eq. **(2)** represents the propagation stage where m and n are the respective exponential powers. The metal loss associated with the recession of the metal for scale formation and caused by internal damages (i.e. oxidation and/or sulphidation) was then obtained with the accurate comparison of pre- and post-exposure cylinder dimensions [2,5]. This analytical method enables a statistical record of metal losses at multiple locations for each sample. The distribution is usually represented in normalized probability plots to better describe the hot corrosion behaviour of the exposed materials [2,5,21,22]. The variability in metal loss data usually observed can be attributed to a distribution in the transition time (t_{inc}). In other words, different locations of the sample can change from incubation stage to propagation stage at different times depending on the local conditions (e.g. gas composition, scale integrity and deposit composition). The precise determination of the incubation lifetimes is therefore of utmost importance to substantiate the corrosion attack of the material. In specific conditions (i.e. for aggressive deposits or susceptible materials), the incubation time is close to zero and the exponentional power n is equal to 1. Consequently, Eq. **(2)** can be written as:

$$ML = k_{prop}.t \quad \textbf{(3)}$$

when the sample shows fast corrosion attack with a linear dependence with time. The internal reactive surface that governs the reaction is assumed to remain constant with time in Eq. ***(3)***.

Up to now, the modelling of hot corrosion damages by means of dimensional metrology has only been developed for nickel-based alloys [2,3,5,21] and ferritic steels [21,22]. Therefore, the present study focuses on modelling the hot corrosion behaviour of pure nickel, the base element of many industrial alloys. The influence of the testing conditions on the mechanisms of hot corrosion of pure nickel at 700°C has already been studied in Ref. [17]. This earlier study highlighted the major influence of pO_2 and pSO_3 and the importance of capillarity effects on the initiation and on the propagation of hot corrosion on pure nickel. The samples half-embedded in Na_2SO_4 and exposed to dry air or to synthetic air + 0.5% SO_2/SO_3 presented complex mechanisms with variable extent of corrosion attack depending on the sample location. The aim of the present study is therefore to correlate the kinetics and the mechanisms of hot corrosion of pure nickel in dry air and in synthetic air + 0.5% SO_2/SO_3 at 700°C, with and without Na_2SO_4, using dimensional metrology method. This method appears particularly helpful to describe the extent of the corrosion attack of nickel and its dispersion and to estimate the corrosion rates in the different testing conditions.

2. Experimental procedure

2.1. Samples preparation

All the tests were conducted on polycrystalline nickel samples with a diameter of 12.7 mm and 2.0 mm thick provided by GoodFellow (99.98 % purity, average grain size of 120 µm). After polishing with SiC P1200, the samples were rinsed with deionized water and accurately measured then cleaned in ethanol and dried again before the hot corrosion tests.

2.2. Hot corrosion tests

The pure nickel samples were exposed to two different atmospheres at 700°C to substantiate the role of SO_2/SO_3 on the hot corrosion mechanisms. Therefore, a first set of samples was exposed just to dry air in a box furnace while synthetic air + 0.5% SO_2 (Air Liquide) flew through iron zeolites catalysators in a horizontal furnace for the second set of samples. The experimental set up has already been described in Ref. [17] and allows the oxidation of SO_2 into SO_3 according to reaction **(4)**:

$$SO_2(g) + \frac{1}{2} O_2(g) \rightleftarrows SO_3(g) \quad \textbf{(4)}$$

The equilibrium pSO_3 of the resulting gas mixture (i.e. synthetic air + 0.5% SO_2/SO_3) was calculated to be $7.5x10^{-3}$ atm at 700°C from data in Ref. [7]. Therefore, liquid Na_2SO_4-$NiSO_4$ should be thermodynamically stable upon reaction of pure nickel with the gas mixture and Na_2SO_4 since the minimum pSO_3 for liquid formation is about $3.0x10^{-4}$ atm at 700°C [23]. To follow the kinetics of hot corrosion of pure nickel, both the half-embedding method [24] and the salt-recoating method were carried out [25]. For the salt-recoating method, Na_2SO_4 is usually deposited by evaporating a saturated solution on preheated samples. The deposit is then periodically refurbished by removing the samples from the furnace, brushing the old deposit and applying a fresh deposit. **Table 1** summarizes the different testing conditions investigated in this study. The Na_2SO_4 powder was provided by Merck (99.0 % purity, average particle size of 45 µm). In condition 1a, pure nickel samples were exposed to synthetic air in a SETARAM TGA 92 thermobalance to constitute a baseline to investigate the oxidation behaviour of pure nickel. In condition 1b, the samples were exposed to synthetic air + 0.5% SO_2/SO_3 in a conventional horizontal furnace. In conditions 2a and 2b, the samples were half-embedded in alumina crucibles containing compacted Na_2SO_4 powder (2.50 g ± 0.02 g of salt for each sample). For all these conditions, the samples were placed in a cold furnace and then heated up to 700°C at 50°C/min. The isothermal corrosion tests were conducted at 700°C for 20, 100 and 300 h. After exposure, the samples were cooled down in the furnace. For the salt-recoating method (conditions 3a-low and 3a-high), sodium sulphate was deposited by evaporating a saturated aqueous solution on a preheated sample [25]. To investigate the influence of the contaminant flux rate on the corrosion attack [1,8], two different deposit loads were applied on the samples (3.0 ± 0.3 $mg.cm^{-2}$ and 20.0 ± 2.0 $mg.cm^{-2}$) and rejuvenated every 20 h. These loads corresponded respectively to the low fluxing rate (0.15 $mg.cm^{-2}.h^{-1}$) and to the high fluxing rate (1.00 $mg.cm^{-2}.h^{-1}$). Each cycle is decomposed as follows: heating of the samples at 50°C/min up to 700°C, isothermal exposure at 700°C for 20 h, removal of the samples from the hot furnace and cooling in air (the time to cool down to 50°C was 15 minutes). After each thermal cycle, the samples were softly brushed to mechanically remove the previous Na_2SO_4 deposit.

Whereas conditions 2a and 2b were specifically designed to investigate the influence of pO_2 and pSO_3 on the mechanisms of hot corrosion of pure nickel [17], such large amounts of salt are not expected to deposit on gas turbine components. With thin deposits of Na_2SO_4, conditions 3a and 3b are therefore closer to real conditions encountered in gas turbine environments and in fireside corrosion. Finally, conditions 1a and 1b simulate the gas-induced hot corrosion observed in the absence of deposit.

Table 1. Summary of the testing conditions investigated in this work. All tests were carried out at 700°C with pure Na_2SO_4.

Testing conditions	Atmosphere	Method	Exposure
1a	Air	Atmosphere only	Isothermal
1b	Air + 0.5% SO_2/SO_3		
2a	Air	Half-embedding	Isothermal
2b	Air + 0.5% SO_2/SO_3		
3a-low (0.15 mg.cm^{-2}.h^{-1}) **3a-high (1.00 mg.cm^{-2}.h^{-1})**	Air	Salt-recoating	Cyclic
3b-low (0.15 mg.cm^{-2}.h^{-1})	Air + 0.5% SO_2/SO_3	Salt-recoating	Isothermal

2.3. Dimensional metrology and modelling of the hot corrosion damages

The aim of the dimensional metrology method (**Fig. 1**) is to accurately describe the local thickness of corroded samples prior and after exposure (i.e. metal loss) to substantiate the extent of the hot corrosion attack [2,4,5]. This metal loss corresponds to the recession of the metal for scale formation and is caused by internal degradation as represented in **Fig. 1**c. The metal recession was measured at multiple locations (60 measurements for each sample) to obtain a statistical record of the metal loss values (**Fig. 1**d). Following the norm ISO 26146:2012 [26] and Ref. [2], the data were then plotted in descending order as a function of the probability of metal loss exceeding value (**Fig. 1**e). Data fitting a Gaussian distribution appear as a straight line whose slope corresponds to the standard deviation of the data set [26]. Any deviation from a straight line indicates a second population and can be interpreted as, e.g. pitting, grain boundary attack or corrosion mitigation.

By measuring the metal loss values at several exposure time, it was thus possible to plot the evolution of the median values over time [2,4,5,27]. Since pure nickel presented very short incubation times and that the evolution of the metal loss values was not directly proportional to time for the testing conditions of this study, the data have been fitted to curves of the type:

$$y = k.t^n + c \qquad \textbf{(5)}$$

Eq. **(*5*)** has been developed by Sumner et al. to model the propagation rates of CMSX-4 superalloy, presenting very short incubation times in Type-II hot corrosion conditions [5]. Depending on the testing conditions (i.e. atmosphere and presence of Na_2SO_4), different lifetime evolutions were described by adjusting the power n required to fit the experimental data. The deviation from linear growth kinetics (i.e. n = 1) can therefore be correlated to the mechanisms

of corrosion of pure nickel and to the thermodynamic conditions. For example, the evolution given in **Fig. 1**f is characteristic of a diffusion controlled corrosion process.

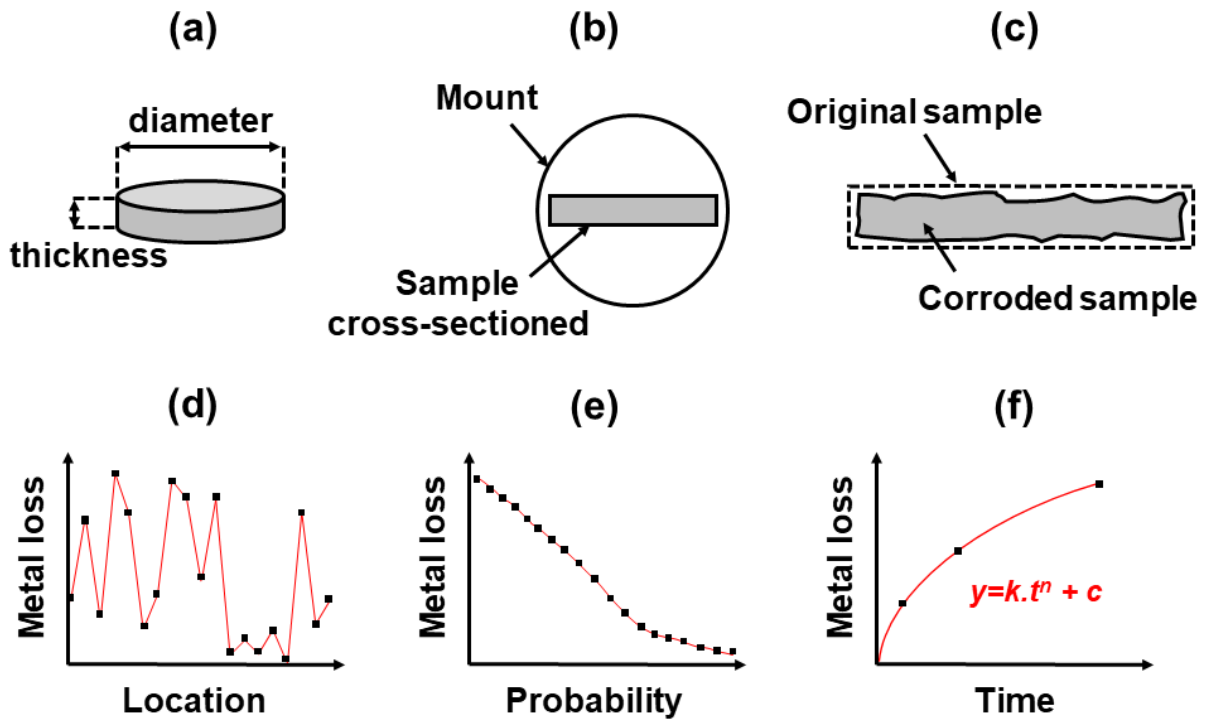

Fig. 1. Dimensional metrology method put in order for the statistical measurements of the hot corrosion of nickel from Ref. [5]: **(a)** sample dimensions measurements before exposure, **(b)** preparation of the sample for the metallographic observation in cross-section after exposure, **(c)** measurements of the residual thickness of the corroded sample on evenly spread locations by optical microscopy (60 measurements for each sample), **(d)** extent of the metal loss compared to the original sample dimensions, **(e)** probability plot of the metal loss measurements for the corroded sample and **(f)** evolution of the metal loss with exposure time and modelling.

2.4. Metallographic examinations

The samples were embedded in epoxy right after the corrosion tests, hence avoiding potential degradation from water moisture. Similarly, the samples were prepared for metallography and further analyses in water-free media [28]. In particular, petroleum oil was employed to polish down to SiC P4000, then in a 1µm diamond suspension and finally cleaned with dry acetone. The cross-sections were observed with a LEICA DM RM/E light optical microscope. Metal loss measurements were performed at 50-fold magnification and recorded with "Imagic IMS" software. For the SEM observations and chemical analyses, a Philips XL40 microscope coupled to an EDAX detector was employed. Raman micro-spectrometry (Jobin Yvon LabRam HR800, λ = 632.82 nm) was also carried out to identify all kinds of inorganic compounds formed upon the tests.

3. Results

3.1. Oxidation

The thermogravimetric analyses (TGA) of pure nickel exposed to synthetic air allowed to investigate the oxide scale formation and plot the oxidation kinetics at 700°C (condition 1a). Under the SEM, the cross-sections displayed a two-layered structure regardless of the oxidation time. The outer scale is columnar while the inner is porous and equiaxed (**Fig. 2**a and b). The overall oxide scale thickness is of approximately 5-6 µm after 20 h of exposure and 10-12 µm after 100 h of exposure. These observations are in good agreement with the works of Peraldi et al. [29,30]. The weight gain curves recorded by TGA are presented in **Fig. 2**c. The parabolic rate constant k_p calculated from the transformed curves is 4.3×10^{-6} $mg^2.cm^{-4}.s^{-1}$, which is in the same range of order than data from literature [30,31]. The determination of the metal loss following **Fig. 1** was not possible for these samples since that the standard deviation of the metrology method (± 10 µm) was greater than the measured values. This is consistent with the overall thickness of the NiO scales formed after 20 h (**Fig. 2**a) and 100 h (**Fig. 2**b).

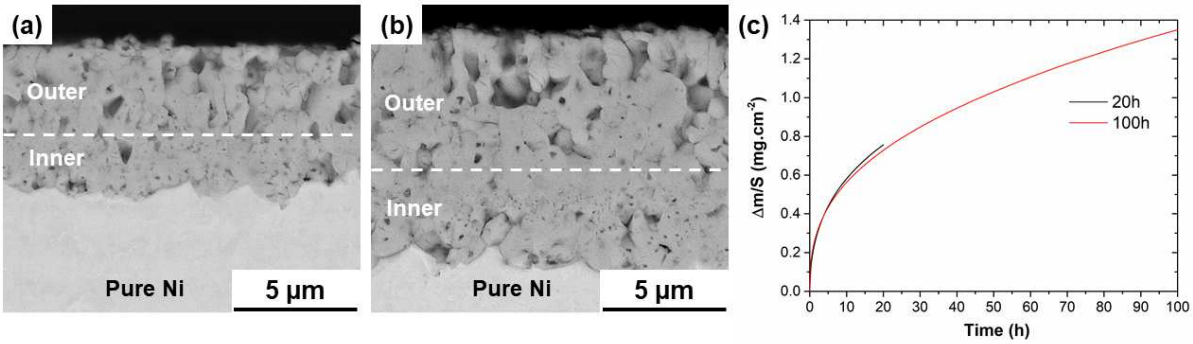

Fig. 2. SEM cross-section images of the nickel oxide scales formed on pure nickel after **(a)** 20 h and **(b)** 100 h of exposure to synthetic air at 700°C and **(c)** corresponding thermogravimetric curves.

3.2. Oxidation-sulphidation

The addition of 0.5% SO_2/SO_3 to synthetic air changed the mechanisms of corrosion of pure nickel switching from pure oxidation to mixed oxidation-sulphidation mechanisms [17]. Whereas a continuous oxide scale formed at the surface after exposure to synthetic air (**Fig. 3**a), mixed corrosion products were formed in the sulphur-containing atmosphere (**Fig. 3**b, c and d). The progressive development of large nodules with time suggests that the presence of SO_2/SO_3 molecules considerably increased the corrosion kinetics of pure nickel. The microstructure of the corrosion scales was examined in cross-section to compare with the oxidized samples (**Fig. 2**). After 20 h of exposure (**Fig. 4**a), a 40 µm thick porous NiO scale had formed above a sulphur-enriched area identified as the Ni_3S_2-Ni eutectic composition. The overall thickness of the corrosion scales increased with time and exhibited a significant roughness after 300 h of

exposure (**Fig. 4**c) as observed on the surface macrographs. Regardless the exposure time (**Fig. 4**), the Ni_3S_2-Ni eutectic mixture was systematically observed at the metal/scale interface and throughout the inner region of the porous NiO scale suggesting the continuous formation of Ni-S liquid solutions at temperature [11,10,32].

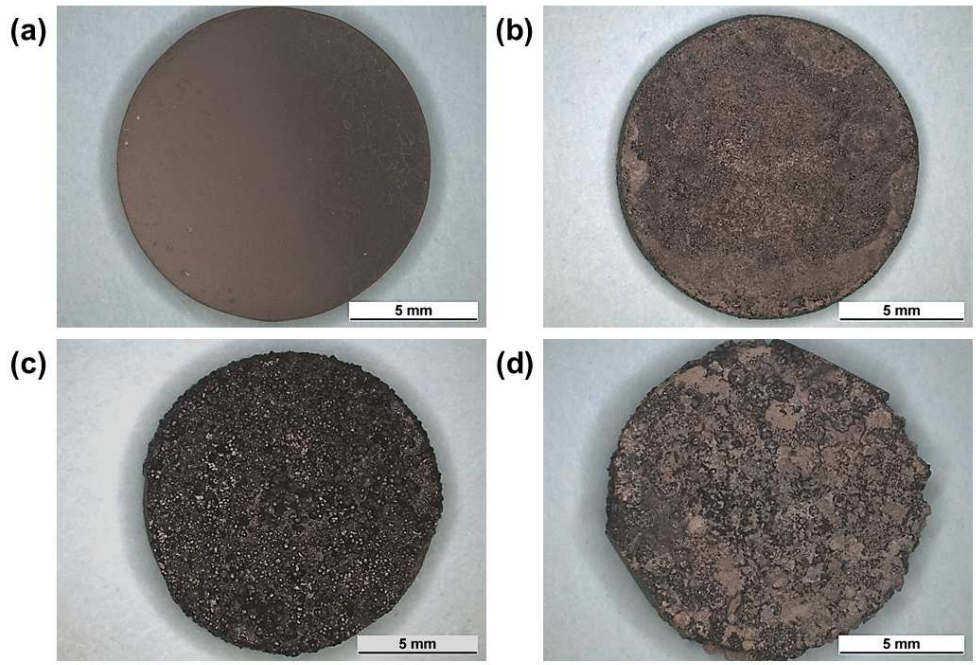

Fig. 3. Surface macrographs of pure nickel samples after exposure for **(a)** 100 h in synthetic air (condition 1a) and for, respectively, **(b)** 20 h, **(c)** 100 h and **(d)** 300 h in synthetic air + 0.5% SO_2/SO_3 (condition 1b) at 700°C.

Insofar as there is at least two products formed when exposing pure nickel to synthetic air + 0.5% SO_2/SO_3, the weight gain measurements are not any longer representative of one mode of corrosion. Therefore, dimensional metrology was conducted to give an accurate profile of the corroded samples and better describe the evolution of the corrosion attack with time [5].

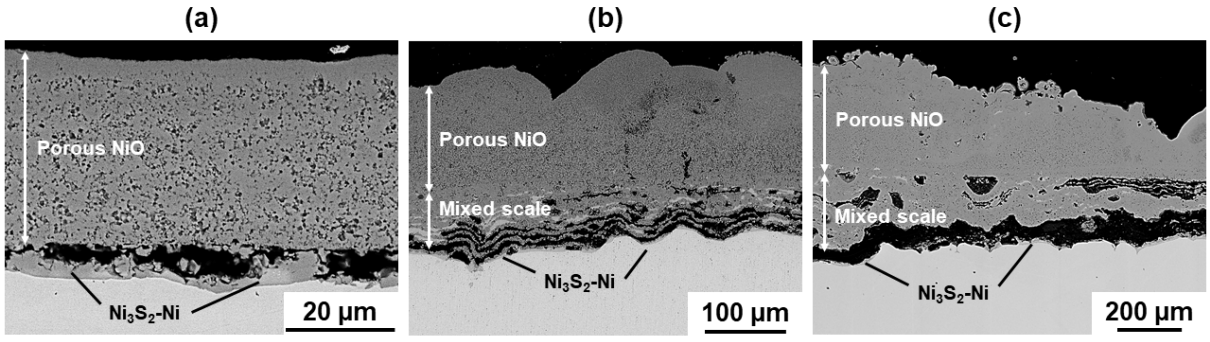

Fig. 4. BSE cross-section images of the scales formed on pure nickel after **(a)** 20 h, **(b)** 100 h and **(c)** 300 h of exposure to synthetic air + 0.5% SO_2/SO_3 at 700°C (condition 1b).

The probability plots of the metal loss measurements for the samples exposed to synthetic air + 0.5% SO_2/SO_3 are given in **Fig. 5**a. On such plots, for each metal loss value, the probability of metal losses greater than this value is calculated [2]. According to **Fig. 5**a, there is 90% probability that the metal losses of pure nickel exceed 31, 96 and 216 µm after, respectively, 20, 100 and 300 h of exposure to condition 1b. For metal losses exceeding 50, 123 and 325 µm after, respectively, 20, 100 and 300 h of exposure in the same condition, the probability drops to 10%. Whereas the experimental data after 100 h of exposure followed a Gaussian distribution, two distributions appeared after 20 and 300 h of exposure (**Fig. 5**a). Following the procedure described in ISO 26146:2012 [26], the slope of the linear fits (i.e. standard deviation of the data set) for each distribution is reported on **Fig. 5**a. As the exposure time increases, the standard deviation values increase suggesting that the corrosion attack is not steady and depends on the local conditions. The appearance of a second distribution with higher metal losses after 20 h and 300 h of exposure can be attributed to more favourable conditions for sulphidation to occur (higher pS_2 and/or higher diffusivity of nickel).

In **Fig. 5**b, the median metal loss values with the maximum and minimum corrosion attack and the values for 10 and 90% of probability have been plotted as a function of the exposure time. The increase in metal loss values is not directly proportional to time and the experimental data have been curve fitted according to Equation **(*5*)** [5]. When exposed to synthetic air + 0.5% SO_2/SO_3, pure nickel exhibited a very short incubation time (less than one hour) showing that the NiO scale does not form a barrier that provides protection to hot corrosion. However, a drop in the corrosion rate is observed with increasing exposure time (n = 0.8).

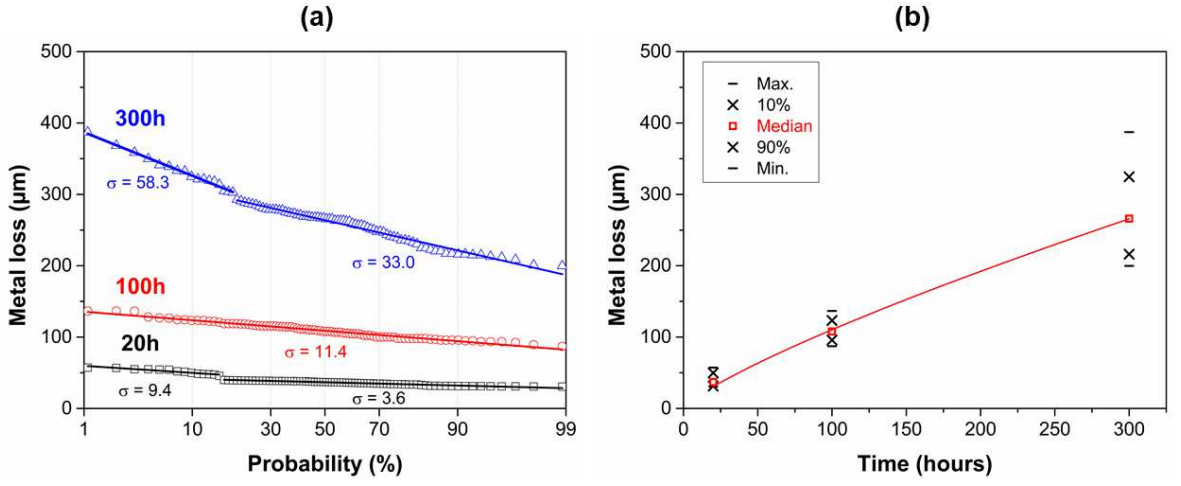

Fig. 5. (a) Probability plots and **(b)** evolution of the metal loss values with time for pure nickel samples exposed to synthetic air + 0.5% SO_2/SO_3 (no Na_2SO_4) at 700°C for 20, 100 and 300 h of exposure (condition 1b).

Pure nickel exposed to synthetic air + 0.5% SO_2/SO_3 at 700°C was further characterized by SEM and presented an equilibration layer of approximately 1 µm thickness at the scale/gas interface after 100 h of exposure (**Fig. 6**a). The correlation between EDS and Raman analyses (**Fig. 6**b) indicates that this layer is composed of $NiSO_4$ and NiO. These results are in good agreement with the surface analyses of pure nickel exposed in the same conditions [17] and with the mechanisms proposed in Refs. [13,15]. This equilibration layer was only observed on pure nickel exposed to condition 1b and confirms that the pSO_3 is high enough in atmosphere b to foster the formation of $NiSO_4$. Very little sulphur was detected in the porous NiO scale underneath the outer $NiSO_4$ + NiO layer.

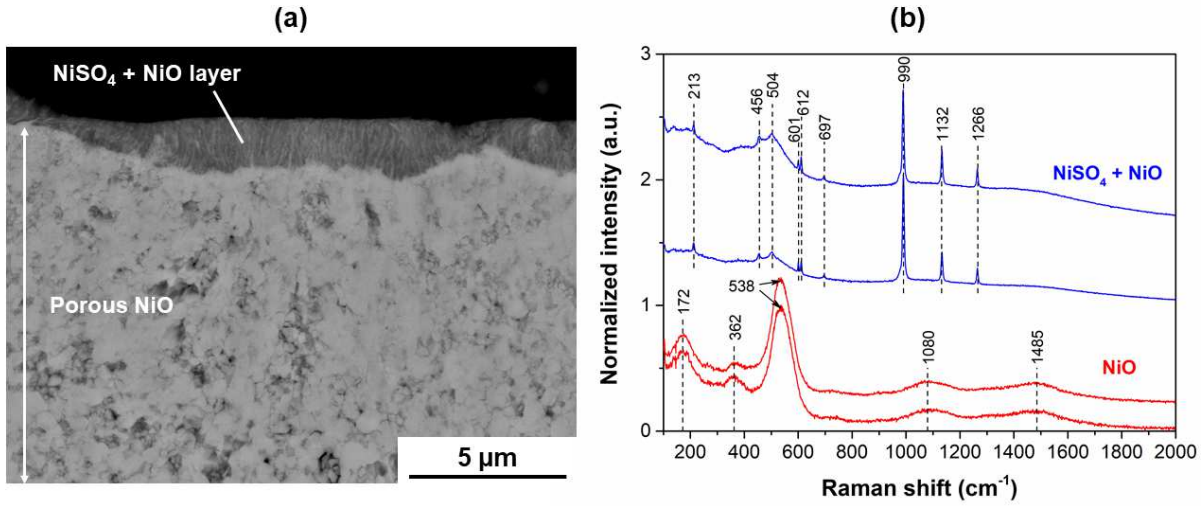

Fig. 6. (a) BSE cross-section image of the scale/gas interface for pure nickel exposed to synthetic air + 0.5% SO_2/SO_3 at 700°C for 100 h and **(b)** corresponding Raman spectra of the dark external layer and of the porous NiO scale.

3.3. Half-embedding in Na_2SO_4

Pure nickel samples half-embedded in Na_2SO_4 were exposed to dry air and synthetic air + 0.5% SO_2/SO_3 at 700°C to investigate the influence of the atmosphere on the extent of the corrosion attack. **Fig. 7** illustrates the microstructure of the corrosion scales for the different testing conditions as a function of time. As previously reported by Gheno and Gleeson [16] and in our group [17], the kinetics of corrosion are significantly higher in the sulphur-containing atmosphere than in dry air. In both atmospheres, the corrosion scales exhibit different microstructures on the atmosphere side and on the salt side (**Fig. 7**). When pure nickel is exposed to dry air, a thin and porous NiO scale together with Ni_3S_2-Ni eutectic at the metal/scale interface are formed on the atmosphere side. On the salt side, mixed Ni_3S_2-Ni + NiO nodules are randomly observed above the porous NiO scale after exposure to dry air, as observed in Refs. [17,33]. One can see the progressive growth of such nodules with increasing exposure time (**Fig.**

7). However, no direct interaction between the growing scales and Na_2SO_4 was observed in dry air.

When pure nickel is exposed to synthetic air + 0.5% SO_2/SO_3, two simultaneous corrosion processes can be observed at both metal/scale and scale/gas interfaces on the atmosphere side (**Fig. 7**). After 20 h of exposure, a thick and continuous porous NiO scale developed on the surface with infiltration of Na_2SO_4-$NiSO_4$ at the scale/gas interface (down to approximately 50 µm within the NiO scale). Similar results were obtained by Gheno and Gleeson in O_2 + 0.1% SO_2/SO_3 [16]. Increasing the exposure time results in the formation of large mixed nodules where sulphides channels (bright phases in Fig. 7) are observed within the porous NiO matrix. This eventually led to the merging of these mixed nodules after 300 h of exposure. Lillerud and Kofstad reported similar microstructures when reacting pure nickel with Na_2SO_4 in 1 atm. O_2 + 4% SO_2 in the range 660-700°C in Ref. [14]. Note that a Na_2SO_4-$NiSO_4$ solution was systematically observed at the scale/gas interface after 100 and 300 h of exposure on the atmosphere side. Regardless of the exposure time sulphidation simultaneously takes place at the metal/scale interface, which most probably increased the outward diffusion rate of nickel cations [34]. The continuous supply of nickel cations would explain in the progressive dissolution of the substrate as observed in the cross-section micrographs (**Fig. 7**).

Considering now pure nickel exposed to synthetic air + 0.5% SO_2/SO_3 on the salt side, no direct interaction was observed between the salt and the growing scales (**Fig. 7**). As the exposure time increases, the progressive sintering of Na_2SO_4 solid particles was observed in the cross-section micrographs. This probably decreased the permeation rate of the gas towards the substrate and led to more reducing conditions at the metal/scale interface [35,36]. The precipitation of nickel particles within the Ni_3S_2 channels observed at the metal/scale interface and within the porous NiO scale suggests that the Ni-S liquid solution disproportionates upon cooling of the samples [10,11,14]. In comparison to the atmosphere side, the inner reaction front (i.e. metal/scale interface) was less steady on the salt side after exposure to synthetic air + 0.5% SO_2/SO_3 at 700°C.

By comparison with the samples exposed to synthetic air (**Fig. 2**) and to synthetic air + 0.5% SO_2/SO_3 (**Fig. 4**), the microstructure of the scales reveals an effect of the nearby presence of Na_2SO_4 on the mechanisms of corrosion on the atmosphere side (**Fig. 7**). For all testing conditions, increasing the exposure time resulted in higher corrosion levels indicating that the corrosion scales were not protective and permeable to corrosive species (i.e. O_2 and SO_2/SO_3).

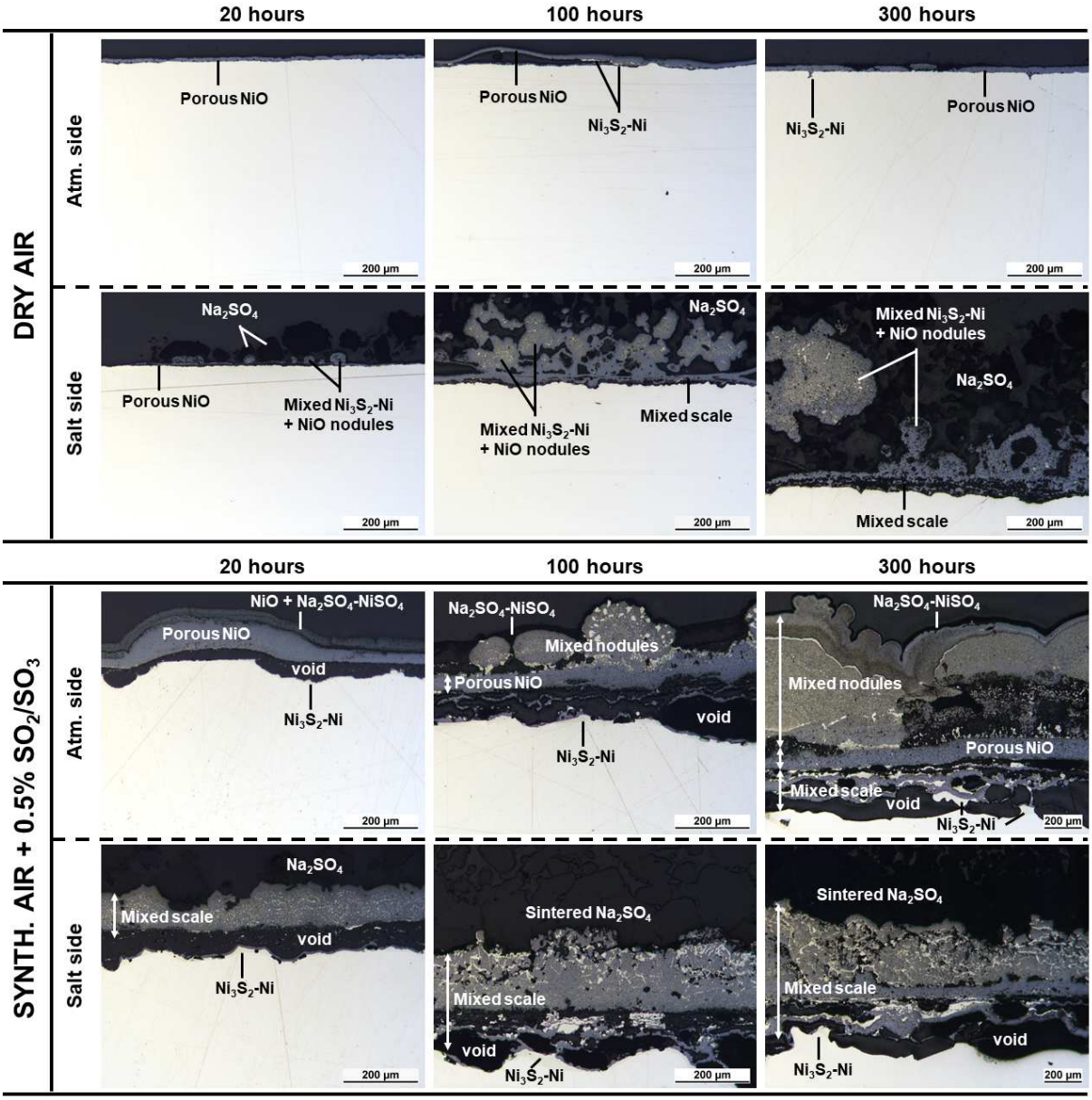

Fig. 7. Cross-section images of the corrosion scales formed on pure nickel half-embedded in Na_2SO_4 and exposed to dry air (condition 2a) or to synthetic air + 0.5% SO_2/SO_3 (condition 2b) at 700°C with time (light optical microscopy).

The probability plots of the metal loss measurements of pure nickel are given in **Fig. 8** for the atmosphere side (no Na_2SO_4) and for the salt side (buried in Na_2SO_4) for 20, 100 and 300 h of exposure. In agreement with the cross-section micrographs of **Fig. 7**, the metal loss increased with increasing exposure time for all conditions. The extent of the corrosion attack was significantly higher in synthetic air + 0.5% SO_2/SO_3 than in dry air (about 6-8 times higher). The standard deviation values for each distribution are reported on the graphs of **Fig. 8** [26]. After 20 h of exposure in dry air, the corrosion profiles of pure nickel are similar on both the atmosphere side and the salt side with standard deviation values of, respectively, 7.2 and 6.3. However, as the exposure time increases, the spread in metal loss values differ for both sides. On

the salt side, the increasing spread of the metal loss values with time can be explained by the progressive accumulation of Ni-S liquid solution at the metal/scale interface leading to cracking of the porous NiO scale (i.e. formation of mixed nodules) and local dissolution of the substrate as observed in **Fig. 7** and in Ref. [33]. On the atmosphere side, two distributions can be observed after 100 and 300 h of exposure. Since the metal loss measurements were conducted on evenly spread areas, this could be explained by a transition between oxidation and sulphidation mechanisms depending on the sample location, namely the local thermodynamic conditions (pO_2 and pSO_3) and the distance between the metal loss measurement and the interfacial region between atmosphere and salt sides. This region is indeed associated with maximum corrosion rates when performing half-embedded experiments [17].

As observed in dry air, the spread of the metal loss values on the salt side increases with increasing exposure time when exposing pure nickel to synthetic air + 0.5% SO_2/SO_3 (**Fig. 8**). This is consistent with the increasing roughness of the inner reaction interface (i.e. metal/scale interface) over time observed in **Fig. 7**. On the atmosphere side, the standard deviation of the experimental data is 29.2 and 29.6 after, respectively, 20 and 100 h of exposure whereas this

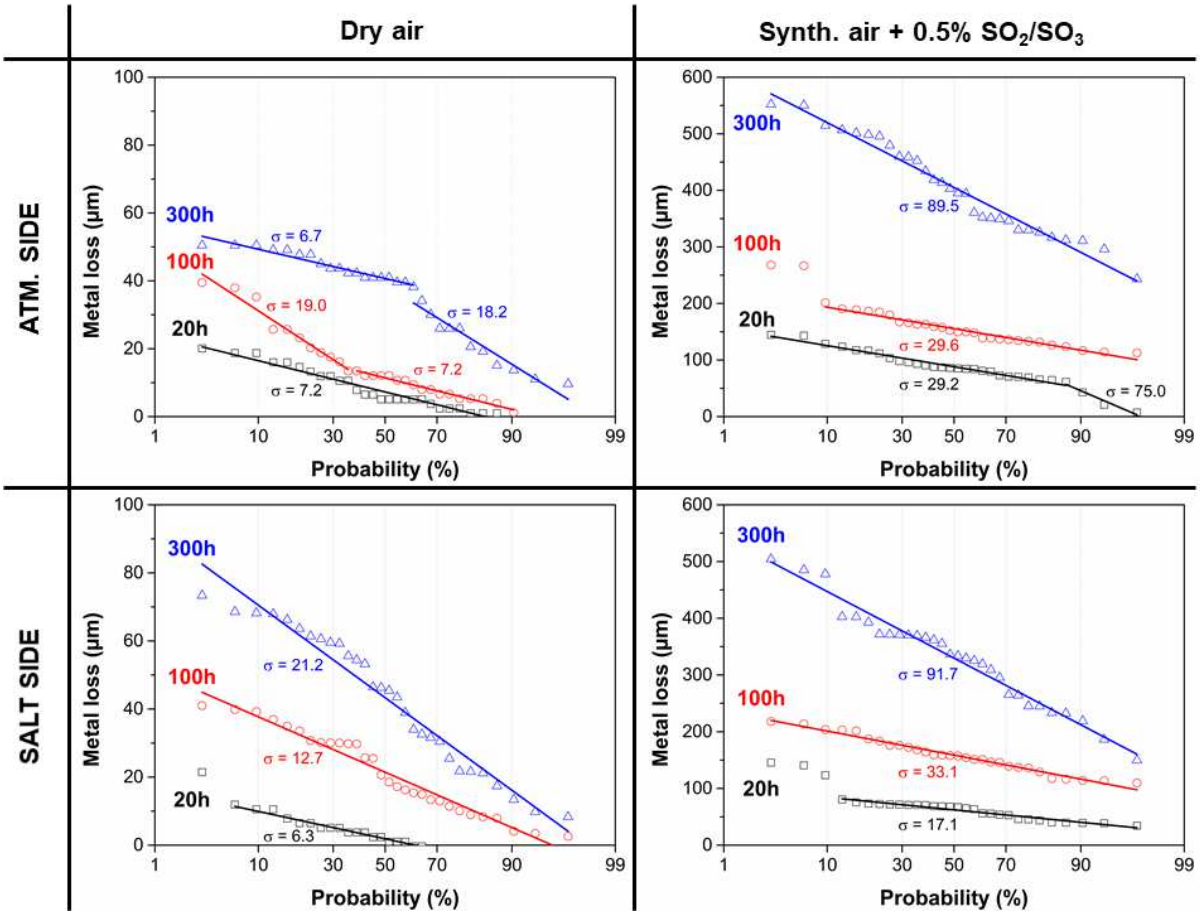

Fig. 8. Probability plots of the metal loss measurements for pure nickel samples half-embedded in Na_2SO_4 and exposed to dry air (condition 2a) and to synthetic air + 0.5% SO_2/SO_3 (condition 2b) at 700°C.

value reaches 89.5 after 300 h of exposure. According to the metal loss measurements, the maximum corrosion attack of pure nickel (approximately 550 µm) occurred on the atmosphere side after 300 h of exposure to synthetic air + 0.5% SO_2/SO_3.

The influence of testing conditions on the evolution of the metal loss values with time is highlighted in **Fig. 9**. The fitted curves indicate that the corrosion kinetics were different between the atmosphere side and the salt side in both atmospheres. Whereas a drop in the corrosion rate is observed on the salt side (*n* values of 0.6 and 0.65 in, respectively, dry air and air + 0.5% SO_2/SO_3), linear corrosion rates are observed on the atmosphere side (*n* = 1). Such differences emphasize the influence of the large Na_2SO_4 reservoir on the corrosion mechanisms (cf. paragraph 4.1.). Note that the median metal loss value is unexpectedly high on the atmosphere side after 20 h of exposure to synthetic air +.0.5% SO_2/SO_3 (**Fig. 9**), i.e. the fitting curve crosses the y-axis for a relatively high metal loss value. This can be explained by the simultaneous sulphidation at the metal/scale interface and Type-II hot corrosion mechanisms (infiltration of Na_2SO_4-$NiSO_4$ liquid solution) at the gas/scale interface as observed in **Fig. 7** and in Refs. [14,16,17]. This results in a high sulphur activity and to very high corrosion rates during

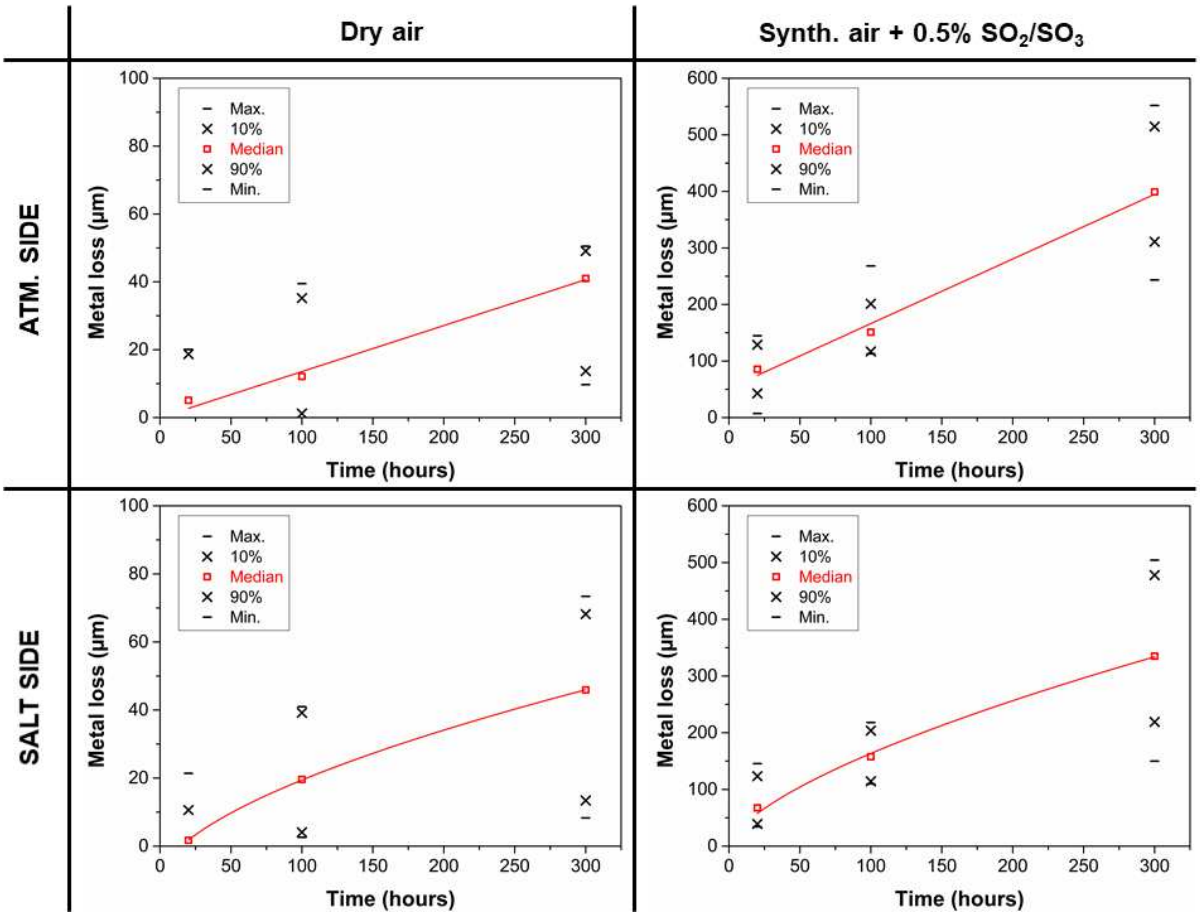

Fig. 9. Evolution of the metal loss values with time for pure nickel samples half-embedded in Na_2SO_4 and exposed to dry air (condition 2a) and to synthetic air + 0.5% SO_2/SO_3 (condition 2b) at 700°C.

the first 20 h of exposure.

3.4. Salt-recoating of Na_2SO_4

The Na_2SO_4 coated samples exposed to dry air at 700°C for 1, 5 and 15 cycles of 20 h, i.e. total exposure time of 20, 100 and 300 h respectively, are shown in **Fig. 10**. For all conditions, the Na_2SO_4 deposits, appearing as dark particles on the light optical micrographs, remained attached to the samples. Nevertheless, no direct interaction occurred between the Na_2SO_4 deposits and the corrosion products as observed in condition 2a (half-embedding in dry air). Regardless the contaminant flux rate and the exposure time, the corrosion scales are not adherent to the metallic substrate and the Ni_3S_2-Ni mixture was systematically observed at the metal/scale interface (**Fig. 10**). Identification of Ni_3S_2-Ni supports that demixing of the Ni-S liquid solution occurred upon cooling [10,11,14]. After 1 cycle of 20 h, spallation of the porous NiO scale is observed in both 3a-low and 3a-high conditions. This might be explained by the rapid cooling rate inducing compressive mechanical stresses due to the CTE (Coefficient of Thermal Expansion) mismatch between Ni and NiO [37,38]. As the exposure time increases, mixed Ni_3S_2-Ni + NiO nodules starts to develop above a relatively continuous NiO scale. After 15 cycles of 20 h, the repeated spallation of the corrosion scales can be observed together with local attack of the substrate (**Fig. 10**). This might indicate the preferential dissolution of the grain boundaries of pure nickel but further characterization should be carried out to validate this hypothesis. A noteworthy observation is that Ni_3S_2-Ni mixtures (bright phases on the micrographs) were systematically observed within the NiO scales. This suggests than capillarity effects play an

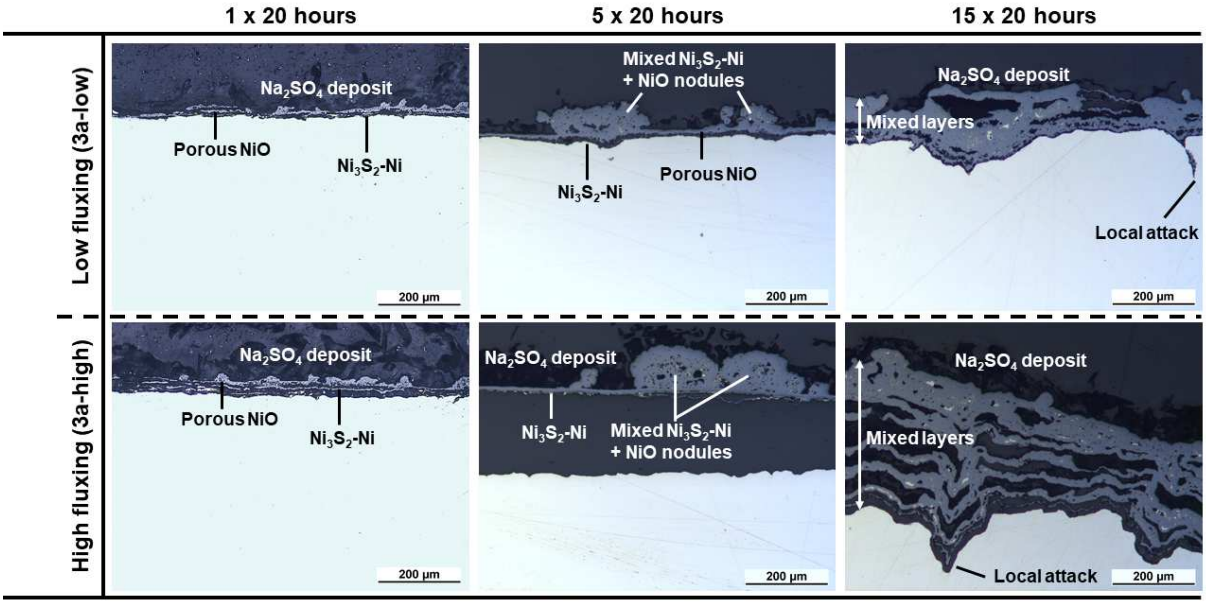

Fig. 10. Cross-section images (light optical microscopy) of the corrosion scales formed on pure nickel coated with Na_2SO_4 after cyclic exposure to dry air at 700°C (low fluxing: 0.15 $mg.cm^{-2}.h^{-1}$ and high fluxing: 1.00 $mg.cm^{-2}.h^{-1}$)

important role in the mechanisms of corrosion as reported earlier by Gheno and Gleeson [16].

The probability plots of the metal loss measurements for the different Na_2SO_4 coated nickel samples are given in **Fig. 11**. As depicted in the cross-section micrographs, a quite uniform corrosion attack (i.e. small standard deviation values) is observed after 1 cycle of 20 h with both low (**Fig. 11**a) and high fluxing (**Fig. 11**b). After 5 cycles of 20 h, a larger spread in the metal loss values is observed and the maximum corrosion attack reaches approximately 60 µm in both fluxing conditions. For the longest exposure, the experimental data do not follow a Gaussian distribution for both low (**Fig. 11**a) and high fluxing (**Fig. 11**b). This can be explained by localized attack of pure nickel substrate fostered by the repeated spallation of the corrosion scales upon cooling. A higher level of corrosion is observed for the higher Na_2SO_4 load after 15 cycles with a maximum corrosion attack of approximately 350 µm.

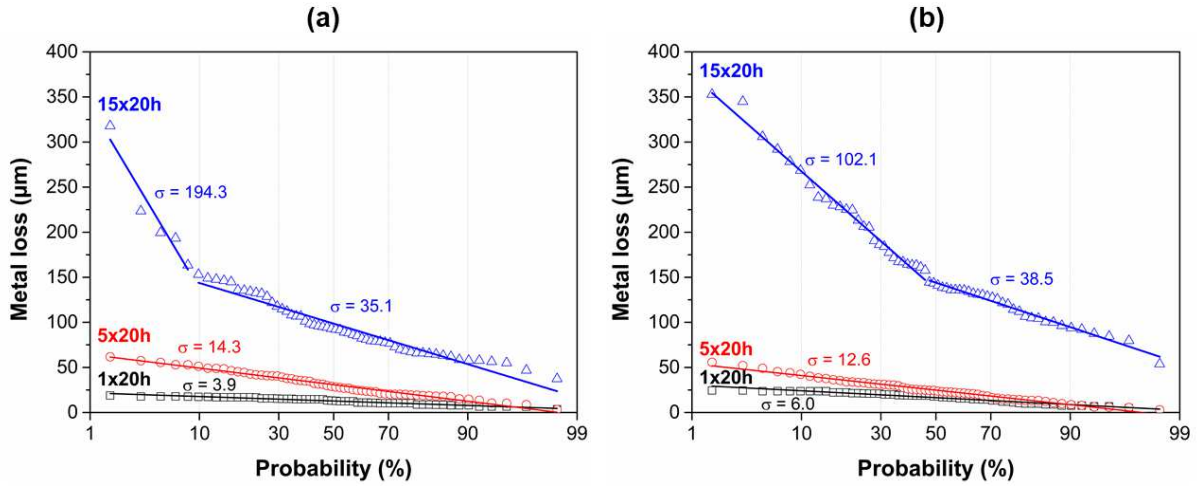

Fig. 11. Probability plots of the metal loss measurements for pure nickel samples submitted to **(a)** condition 3a-low and **(b)** condition 3a-high in dry air at 700°C for 1, 5 and 15 cycles of 20 h.

The evolution of the median metal loss values for the samples exposed to condition 3a-low and condition 3a-high are given, respectively, in **Fig. 12**a and **Fig. 12**b. For both fluxing rates the kinetics are not linear and the corrosion rate increases with increasing exposure time (i.e. increasing number of thermal cycles). It appeared that the higher fluxing rate increased the corrosion rate of pure nickel as observed by Nicholls et al. when reacting CMSX-4 superalloy with SO_x-containing atmospheres and Na_2SO_4-K_2SO_4 mixed deposits [2].

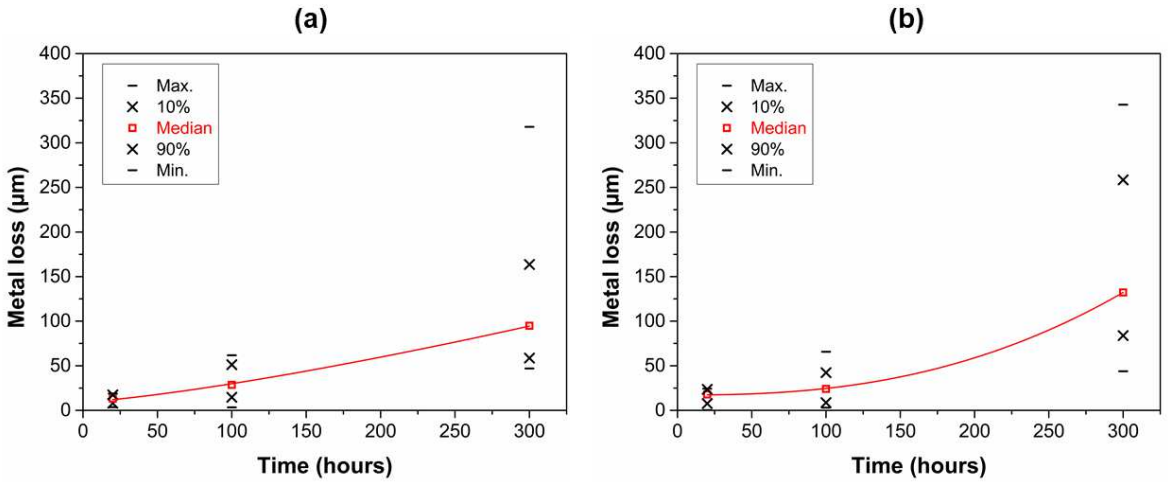

Fig. 12. Evolution of the metal loss values with time for pure nickel samples submitted to **(a)** condition 3a-low and **(b)** condition 3a-high in dry air at 700°C.

Pure nickel was also coated with Na_2SO_4 and exposed to synthetic air + 0.5% SO_2/SO_3 for 100 h isothermally (condition 3b-low in **Table 1**). A BSE cross-section image of a representative area of the sample is given in **Fig. 13**a. The corrosion scale shows a thick and porous NiO scale with dispersed nickel sulphides. The inner region of the scale and the inner reaction front (i.e. metal surface) were enriched with Ni_3S_2-Ni mixtures. Ni_3S_2 also formed within the nickel substrate in highly reducing environments [35,36]. At the scale/gas interface, a mixed Na_2SO_4-$NiSO_4$ layer typical for Type-II hot corrosion mechanisms [16] was systematically observed (**Fig. 13**a). The formation of Ni_3S_2 islands at the scale/sulphate interface suggests that the sulphate layer considerably increased the sulphur activity as proposed by Kofstad et al. [13,14]. The comparison of the cumulative probability plots given in **Fig. 13**b indicates that condition 2b (half-embedding) was more severe than both condition 1b (atmosphere only) and condition 3b-

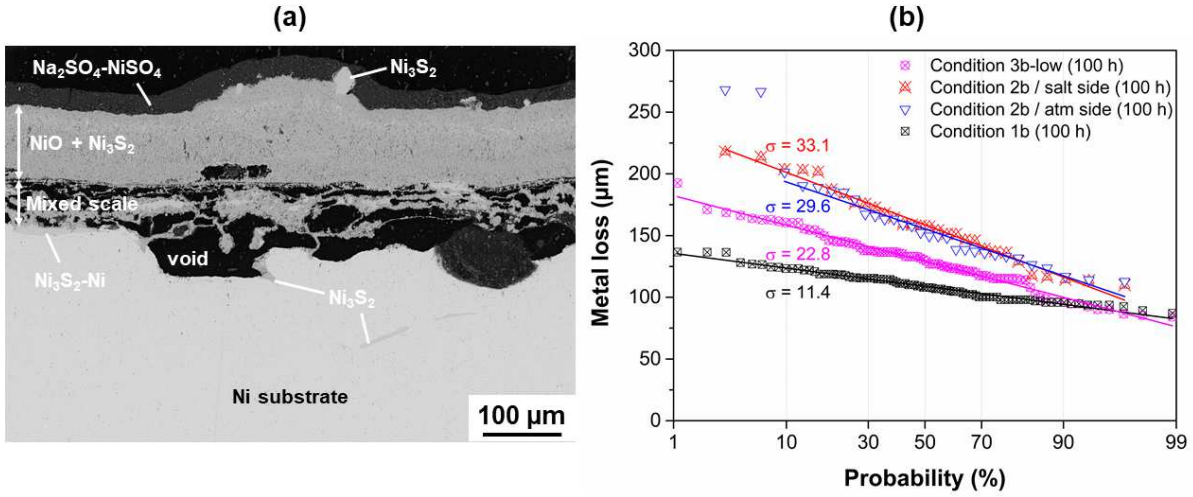

Fig. 13. (a) BSE cross-section image of pure nickel exposed to condition 3b-low for 100 h at 700°C and **(b)** comparison of the probability plots of pure nickel exposed to conditions 1b, 2b and 3b-low for 100 h at 700°C.

low. **Fig. 13**b also indicates that the presence of Na_2SO_4 is associated with a larger spread in the metal loss values by comparison with the experimental data obtained in condition 1b.

4. Discussion

4.1. Correlations between the kinetics and the mechanisms of hot corrosion of pure nickel

The propagation rates (noted k_{prop}) estimated from the dimensional metrology method and the *n* values used to fit the experimental data (median metal loss values) for the different testing conditions have been reported in **Fig. 14**. In synthetic air (with no SO_2/SO_3), pure nickel underwent oxidation with the progressive growth of a *duplex* NiO scale (**Fig. 2**) and shows a low corrosion rate. The addition of 0.5% SO_2/SO_3 to synthetic air considerably increased the kinetics of corrosion with a propagation rate of approximately 0.72 $\mu m.h^{-1}$. This confirms that corrosion scales without Cr or other more resistant oxides formed on nickel alloys are never protective under sulphidizing attack and that the permeation of sulphur-bearing molecules through the physical defects of the scales is responsible of the corrosion attack [9,13]. The local reducing conditions at the metal/scale interface [35,36] fosters the reduction of SO_2/SO_3 molecules into S_2 that progressively reacts with nickel. The systematic identification of Ni_3S_2-Ni mixtures at the metal/scale interface and within the porous NiO scale (**Fig. 4**) confirms that oxidation-sulphidation mechanisms involves the formation of liquid phases at 700°C (Ni-S eutectic at 635°C [11,13,14,32]). This results in the increased diffusivity of both nickel and sulphur and to the fast dissolution of the metallic substrate with time (cf. **Fig. 5**b). The rapid outward diffusion

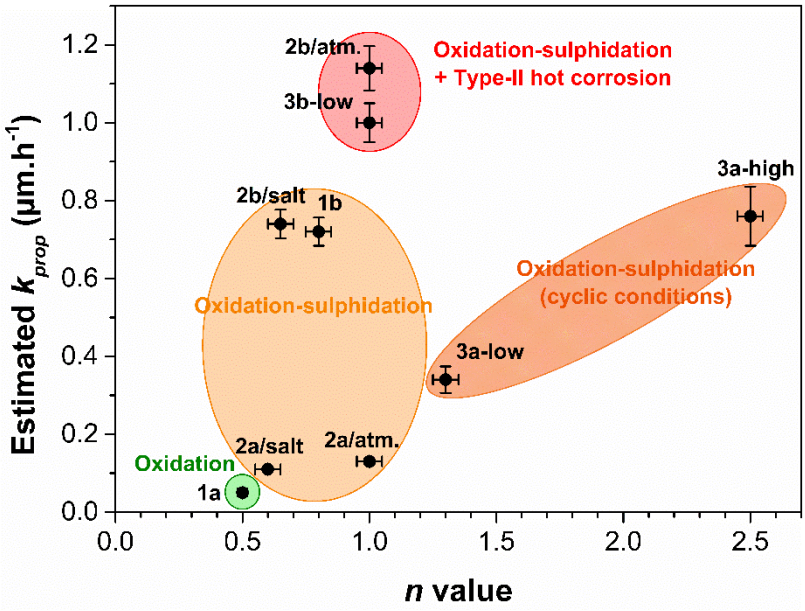

Fig. 14. Corrosion map representing the estimated k_{prop} as a function of the *n* values used to fit the experimental data for pure nickel exposed to the different testing conditions at 700°C. Atmosphere a: air, atmosphere b: air + 0.5% SO_2/SO_3. For condition 3b-low, the *n* value was estimated to be 1.0.

of nickel cations results in the formation of thick and porous corrosion scales with poor adherence to the metallic substrate (**Fig. 4**) and in the formation of $NiSO_4$ at the scale/gas interface as proposed in Refs. [11,13,15,39]. However, a drop in the corrosion rate is observed with increasing exposure time (n = 0.8) in condition 1b (**Fig. 5**b). A similar evolution has been described by Sumner et al. when exposing CMSX-4 superalloy to a mixture of Na_2SO_4-K_2SO_4 at 700°C [5]. Sumner et al. explained this phenomenon as the increasing thickness of the corrosion scale with increasing exposure time, which decreases the diffusion rate of the reactive species towards the substrate.

For the samples half-embedded in Na_2SO_4 (conditions 2a and 2b), the composition of the atmosphere was found to considerably modify the corrosion kinetics of pure nickel (**Fig. 14**). When buried in Na_2SO_4 and exposed to dry air (condition 2a/salt), the samples presented mixed NiO + Ni_3S_2-Ni nodules formed above a continuous oxide scale. Such nodule formation has already been described in Ref. [17] and was associated with the shielding effect of Na_2SO_4 that decreases both pO_2 and pSO_3 at the sample surface (i.e. reducing conditions [35,36]) and to the decomposition of Na_2SO_4 releasing some SO_3 [16]. The evolution of the metal loss values with time (**Fig. 9**) indicates a significant drop of the corrosion rate (n = 0.6). This can be explained by the progressive growth of the mixed nodules, which reduces the permeation rate of the reactive species towards the metal/scale interface [5]. On the atmosphere side (condition 2a/atm.), Ni_3S_2-Ni mixtures were systematically observed at the metal/scale interface and through the porous NiO scales suggesting that Ni-S liquid solutions progressed by capillarity on the sample surface. This is consistent with the comparable propagation rates on both the atmosphere side (0.13 µm.h^{-1}) and the salt side (0.11 µm.h^{-1}) indicating that the whole surface of the samples was prone to oxidation-sulphidation mechanisms.

The half-embedded samples exposed to air + 0.5% SO_2/SO_3 (atmosphere b) present greater corrosion damages (**Fig. 7**) and higher corrosion rates (**Fig. 14**) than the samples exposed to dry air. This is mainly attributed to the greater SO_3 activity in the gas phase, which increases the driving force for sulphidation to occur as observed by Kofstad and co-workers [10,11]. Regardless of the sample region, Ni_3S_2-Ni mixtures were systematically identified at the metal/scale interface and within the porous NiO scales (**Fig. 7**), indicating that the whole sample was prone to sulphidation and covered with a Ni-S liquid solution at 700°C [10,11,14]. On the salt side (condition 2b/salt), the progressive sintering of Na_2SO_4 salt particles is observed on the cross-section micrographs with increasing exposure time. This results in highly-reducing conditions (i.e. high pS_2) [35,36] and to the formation of corrosion scales with a high-volume fraction of sulphides (appearing bright on the cross-section micrographs of **Fig. 7**). With a n value of 0.65 (**Fig. 14**), sintering of Na_2SO_4 particles and thickening of the corrosion scales

considerably limited the diffusion of reactive species towards the substrate. Since no interaction was observed between the corrosion scales and Na_2SO_4 on the salt side, the corrosion attack was mostly attributed to the sulphidation of pure nickel. On the atmosphere side (condition 2a/atm.), the simultaneous oxidation-sulphidation and Type-II hot corrosion of nickel can be observed [16,17]. The formation of liquid Na_2SO_4-$NiSO_4$ solutions at the scale/gas interface increased the sulphur activity within the scales and most likely increased the permeation rate of reactive species towards the substrate [14]. This would explain the higher *n* value used to fit the experimental data in this condition (**Fig. 14**). This resulted in thicker corrosion scales and a higher corrosion rate on the atmosphere side (1.14 $\mu m.h^{-1}$) than on the salt side (0.74 $\mu m.h^{-1}$), as depicted in **Fig. 9**.

Note that large voids systematically formed at the metal/scale interface after the corrosion tests (**Fig. 7**). This may result from a volume change upon decomposition of the Ni-S liquid solution into the eutectic Ni_3S_2-Ni [11,14] and/or from the differences in coefficients of thermal expansion of the different compounds. Both features would induce mechanical stresses and shrinkage of the scales upon cooling to room temperature.

4.2. Influence of the testing conditions on the kinetics of hot corrosion of pure nickel

The influence of the testing conditions on the mechanisms of hot corrosion of pure nickel has already been investigated in our previous work [17]. Based on available thermodynamic data and literature the major influence of both pO_2 and pSO_3 on the development of sulphidation and of Type-II hot corrosion mechanisms was highlighted. The present study also demonstrates that the testing conditions have a strong influence on the kinetics of corrosion of pure nickel (**Fig. 15**).

For all testing conditions the metal loss values increase with increasing exposure time (**Fig. 15**), which indicates that NiO never forms a protective barrier at 700°C. Excluding condition 1a (synthetic air only), sulphidation was observed in all testing conditions. The systematic observation of Ni_3S_2-Ni mixtures at the metal/scale interface indicates that a Ni-S liquid solution formed during the hot corrosion experiments [10,11,14]. Sulphidation was attributed to the molecular transport of SO_2/SO_3 molecules through NiO scales and their reduction into S_2 at the metal/scale interface. Therefore, the spread in the sulphidation attack can be associated with the diffusion rate of the reactive species (i.e. kinetics) and the driving force for sulphidation to occur (i.e. thermodynamics, pS_2 at the metal/scale interface). The results presented in Figs. 14 and 15 confirm this hypothesis, where both addition of 0.5% SO_2/SO_3 and/or Na_2SO_4 to air increased the sulphidation rate of pure nickel. Similar conclusions were given by Gheno and Gleeson in Ref. [16].

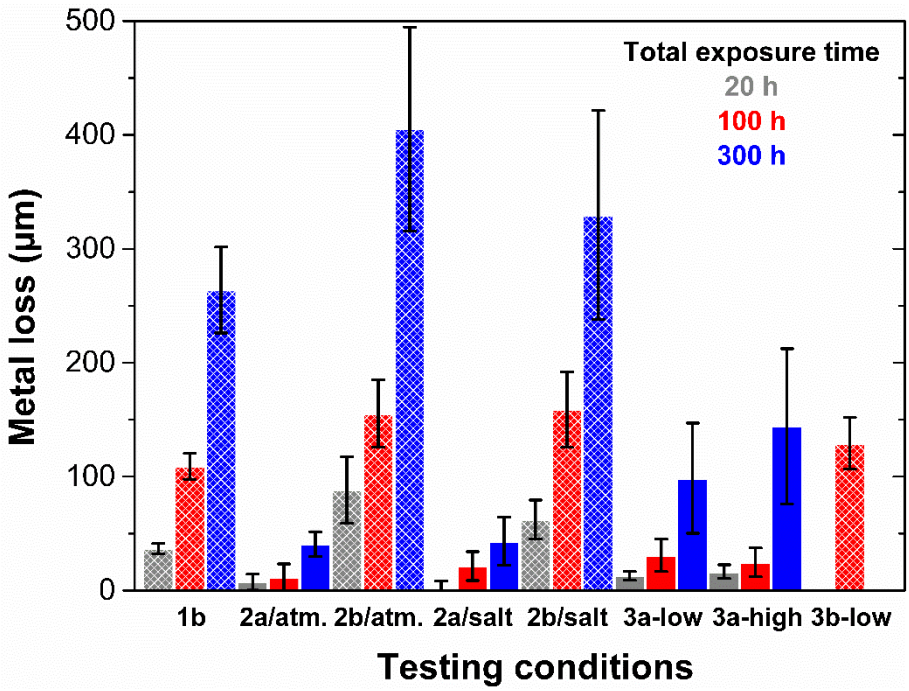

Fig. 15. Summary of median metal loss measurements (with standard deviation) for pure nickel samples exposed to the different testing conditions at 700°C for a total exposure time of 20, 100 and 300 h. Note that only the data after 100 h exposure is presented for condition 3b-low.
Low fluxing: 0.15 $mg.cm^{-2}.h^{-1}$ and high fluxing: 1.00 $mg.cm^{-2}.h^{-1}$.

The comparison of the hot corrosion damages of pure nickel after 100 h of exposure presented in **Fig. 13**b underlines the influence of Na_2SO_4 on the kinetics of corrosion. Whereas a relatively flat corrosion profile is observed when pure nickel is exposed to condition 1b, a larger spread in the metal loss values is observed with addition of Na_2SO_4. Note that the volume fraction of sulphide phases within the corrosion scales is much higher when using the half-embedding method (**Fig. 7**) than the salt-recoating method (**Fig. 13**a) in air + 0.5% SO_2/SO_3. This was attributed to the greater amount of Na_2SO_4 deposited on the sample. Whereas an infinite reservoir of Na_2SO_4 was present for the half-embedding method (approximately 1940 $mg.cm^{-2}$), about 30 $mg.cm^{-2}$ was deposited on the samples for condition 3b. Therefore, Na_2SO_4 exerts a shielding effect by decreasing the permeation of the gas reactive species (i.e. O_2 and SO_2/SO_3 molecules) and by maintaining a relatively high pS_2 at the metal/scale interface and within the scale [16,17]. As forecasted in Refs. [35,36], thick salt deposits result in the stabilization of sulphides at the metal/scale interface because of more reducing conditions (i.e. higher pS_2). This results in higher sulphidation kinetics.

The higher metal loss values recorded in condition 2b/atm. side than in condition 2b/salt side (**Fig. 15**) can be attributed to the simultaneous formation of the Na_2SO_4-$NiSO_4$ eutectic solution at the scale/gas interface on the atmosphere side (**Fig. 7**). As reported by Gheno and Gleeson [16] and in Ref. [17], the liquid Na_2SO_4-$NiSO_4$ solution first permeated the porous NiO scale and

eventually covered the scale since fresh Na_2SO_4 was still available with the half-embedding method. The evidence of mixed Na_2SO_4-$NiSO_4$ in the corrosion microstructures was generally not observed in O_2 + 4% SO_2/SO_3 since Na_2SO_4 was the limiting reagent [10,14].

For the salt-recoating method, two important parameters must be considered: the influence of thermal cycling on the adherence of the corrosion scales and the influence of the contaminant flux rate (CFR) given in $mg.cm^{-2}.h^{-1}$ [1,8]. For both half-embedded and salt-recoated samples exposed to dry air, the same mechanisms of corrosion were observed (i.e. oxidation-sulphidation with formation of mixed NiO + Ni_3S_2-Ni nodules). Nevertheless, the thermally-induced stresses caused by the repeated cycles fostered the spallation of the corrosion scales in the salt-sprayed samples. This was highlighted on the cross-section micrograph after 15 cycles of 20 h with the high fluxing (**Fig. 10**). This considerably decreased the adherence of the corrosion scales and hence increased the corrosion rate of pure nickel. After 5 cycles of 20 h, the contaminant flux rate did not show a significant difference in the corrosion attack as observed by metallographic examination (**Fig. 10**) and by metrology (**Fig. 11**). This was no longer true after 15 cycles of 20 h where the samples exposed to the higher fluxing exhibited higher levels of corrosion with a propagation rate and *n* value approximately 2 times higher than the samples exposed to the low fluxing (**Fig. 14**). The same trend was observed for coated and uncoated nickel-based superalloys exposed to burner rig tests [2,8,40]. Note that the repeated spallation of the corrosion scales also changes the thermodynamic conditions at the metal/scale interface (e.g. pO_2 and pS_2) resulting in alternative oxidation and sulphidation mechanisms. The formation of a Ni-S liquid solution at the metal/scale interface and its further decomposition upon cooling as a mixture of Ni_3S_2-Ni could also play a role on the low adherence of the scales to the metallic substrate. Therefore, the relatively high *n* value for condition 3a-high (**Fig. 14**) can be ascribed to a synergistic effect between the decomposition of the Ni-S eutectic melt and the differences in coefficients of thermal expansion of the compounds, inducing mechanical stresses and shrinkage of the scales upon cooling to room temperature.

5. Conclusions

Based on the correlations between the kinetics and the mechanisms of hot corrosion of pure nickel, the following conclusions can be drawn:

1. The access of sulphur-bearing molecules to pure nickel through the physical defects of the growing oxide scales considerably increased the corrosion kinetics of pure nickel with the formation of Ni-S eutectic melt at the metal/scale interface.
2. Regardless of the testing method (half-embedding or salt-recoating), Na_2SO_4 accelerated the sulphidation of pure nickel because of a shielding effect, which fostered the dissociation of SO_2/SO_3 into S_2 (i.e. reducing conditions).
3. For longer exposure time (300 h), thermal cycling played a significant role on the corrosion attack by fostering the spallation of the corrosion scales. A synergistic effect between the differences in coefficients of thermal expansion of the compounds and the decomposition of Ni-S liquid solution into Ni_3S_2-Ni was proposed.
4. The contaminant flux rate was also found to influence the corrosion kinetics without modifying the mechanisms of corrosion.
5. When pure nickel was exposed to synthetic air + 0.5% SO_2-SO_3 and Na_2SO_4, sulphidation and Type-II hot corrosion mechanisms were simultaneously observed. Since both mechanisms contribute to the corrosion kinetics, it is important to carefully design the hot corrosion experiments.

Acknowledgments

The authors gratefully acknowledge the French Ministry of Armed Forces (Direction Générale de l'Armement) for funding this research (Grant no. 2014.60.0059).

References

[1] P. Hancock, Corros. Sci. **22** (1982) 51-65.

[2] J.R. Nicholls, N.J. Simms, A. Encinas-Oropesa, Mater. High Temp. **24** (2007) 149-162.

[3] J. Sumner, A. Encinas-Oropesa, N.J. Simms, J.E. Oakey, Mater. High Temp. **28** (2011) 369-376.

[4] J. Sumner, A. Encinas-Oropesa, N.J. Simms, J.E. Oakey, Mater. Sci. Technol. **29** (2013) 813-821.

[5] J. Sumner, A. Encinas-Oropesa, N.J. Simms, J.R. Nicholls, Mater. Corros. **65** (2014) 188-196.

[6] J. Stringer, Mater. Sci. Technol. **3** (1987) 482-493.

[7] F.S. Pettit, Oxid. Met. **76** (2011) 1-21.

[8] S.R.J. Saunders, J.R. Nicholls, Mater. High Temp. **13** (1995) 115-120.

[9] M.C. Pope, N. Birks, Oxid. Met. **12** (1978) 173-181.

[10] P. Kofstad, G. Akesson, Oxid. Met. **12** (1978) 503-526.

[11] M. Seiersten, P. Kofstad, Corros. Sci. **22** (1982) 487-506.

[12] P. Kofstad, G. Akesson, Oxid. Met. **14** (1980) 301-323.

[13] K.P. Lillerud, B. Haflan, P. Kofstad, Oxid. Met. **21** (1984) 119-134.

[14] K.P. Lillerud, P. Kofstad, Oxid. Met. **21** (1984) 233-270.

[15] F. Gesmundo, D.J. Young, S.K. Roy, High Temp. Mater. Process. **8** (1989) 149-180.

[16] T. Gheno, B. Gleeson, Oxid. Met. **84** (2015) 567-584.

[17] B. Grégoire, X. Montero, M.C. Galetz, G. Bonnet, F. Pedraza, Corros. Sci. **141** (2018) 211-220.

[18] C.S. Giggins, F.S. Pettit, Hot Corrosion Degradation of Metals and Alloys: A Unified Theory, PWA Report FR-11545 (1979).

[19] F.S. Pettit, G.H. Meier, Fifth International Symposium, Superalloys Proceedings Archive (1984) 651-687.

[20] N. Birks, G.H. Meier, F.S. Pettit, Introduction to the High-Temperature Oxidation of Metals, Cambridge University Press (2006).

[21] X. Montero, M.C. Galetz, Oxid. Met. **83** (2015) 485-506.

[22] X. Montero, M.C. Galetz, Surf. Coat. Technol. **304** (2016) 211-221.

[23] A.K. Misra, D.P. Whittle, W.L. Worrell, J. Electrochem. Soc. **129** (1982) 1840-1845.

[24] International Standard ISO 17248:2015, Corrosion of metals and alloys – Test method for high temperature corrosion testing of metallic materials by embedding in salt, ash or other solids, 2015.

[25] International Standard ISO 17224:2015, Corrosion of metals and alloys – Test method for high temperature corrosion testing of metallic materials by application of a deposit of salt, ash, or other substances, 2015.

[26] International Standard ISO 26146:2012, Corrosion of metals and alloys – Method for metallographic examination of samples after exposure to high-temperature corrosive environments, 2012.

[27] X. Montero, M.C. Galetz, Oxid. Met. **89** (2018) 499-516.

[28] K. Rahts, M. Schorr, C. Schwaln, M. Schütze, Water-free Methods of Preparation for the Analyses of Chlorides in the High Temperature Oxidation in Chloride Containing Atmospheres, Prakt. Metallogr. **36** (1999) 86-97.

[29] R. Peraldi, D. Monceau, B. Pieraggi, Oxid. Met. **58** (2002) 249-273.

[30] R. Peraldi, D. Monceau, B. Pieraggi, Oxid. Met. **58** (2002) 275-295.
[31] S. Chevalier, F. Desserrey, J.P. Larpin, Oxid. Met. **64** (2005) 219-234.
[32] P. Kofstad, G. Akesson, Oxid. Met. **13** (1979) 57-76.
[33] M.G. Hocking, P.S. Sidky, Corr. Sci. **27** (1987) 205-214.
[34] S. Mrowec, K. Przybylski, Oxid. Met. **23** (1985) 107-139.
[35] V. Lemoine, P. Steinmetz, B. Roques, C. Duret, Corr. Sci **25** (1985) 431-447.
[36] R. Morbioli, P. Steinmetz, C. Duret, Mater. Sci. Eng. **87** (1987) 337-344.
[37] C. Liu, A.M. Huntz, J.L. Lebrun, Mater. Sci. Eng. A **160** (1993) 113-126.
[38] A.M. Huntz, C. Liu, M. Kornmeier, J.L. Lebrun, Corr. Sci. **35** (1993) 989-997.
[39] S.P. Mehandru, A.B. Anderson, J. Electrochem. Soc. **133** (1986) 828-832.
[40] N.J. Simms, A. Encinas-Oropesa, J.R. Nicholls, Mater. Sci. Forum **461-464** (2004) 941-948.